ACS APPLIED MATERIALS & INTERFACES

Research Article

www.acsami.org

Band Alignment for Rectification and Tunneling Effects in Al_2O_3 Atomic-Layer-Deposited on Back Contact for CdTe Solar Cell

Yantao Su,[†] Chao Xin,[†] Yancong Feng, Qinxian Lin, Xinwei Wang, Jun Liang, Jiaxin Zheng, Yuan Lin, and Feng Pan*

School of Advanced Materials, Peking University, Peking University Shenzhen Graduate School, Shenzhen 518055, China

Supporting Information

ABSTRACT: The present work intends to explain why ultrathin Al_2O_3 atomic-layer-deposited (ALD) on the back contact with rectification and tunneling effects can significantly improve the performance of CdTe solar cells in our previous work [Liang, J.; et al. *Appl. Phys. Lett.* **2015**, *107*, 013907]. Herein, we further study the mechanism through establishing the interfacial energy band diagram configuration of the ALD Al_2O_3/Cu_xTe by experiment of X-ray photoelectron spectroscopy and first-principles calculations and conclude to find the band alignment with optimized layer thickness (about 1 nm ALD Al_2O_3) as the key factor for rectification and tunneling effects.

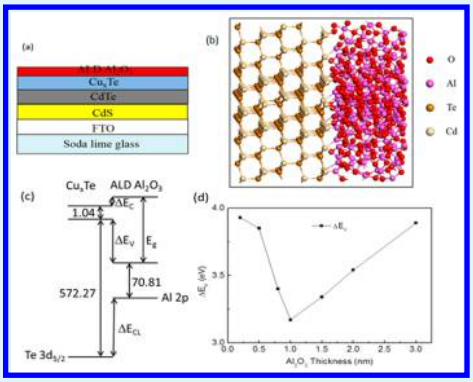

KEYWORDS: *atomic layer deposition, Al_2O_3, band alignment, back contact, CdTe solar cell*

1. INTRODUCTION

Although Si-based solar cell devices currently dominate photovoltaic power production, thin-film solar cell devices based on CdTe have achieved a notable market share as a cost-effective alternative.[1−3] For thin-film CdTe solar cells, efficiency improvement is always the main goal. Generally, the common methods for improving efficiencies include designing new device structures,[4−6] improving the material composition and related crystalline quality of thin films,[7,8] and optimizing the contact interfaces between thin films.[9−11] The back contact is a key issue for the performance of CdTe thin-film solar cells because it is challenging to attain low resistance and a stable electrical contact.[12−17] Many efforts have been devoted to optimize the back contact based on physical concepts and nanoengineering.[18−20]

Recently, Al_2O_3 is a promising candidate to passivate p-type silicon (Si) material because of its good chemical and field-effect passivation.[21−24] In addition, Al_2O_3 is also a good modification material for CdTe, because the lattice mismatch is only 3.7% between the surface of Al_2O_3(0001) and CdTe-(111).[25] In our previous work, we have fabricated a nanostructured back contact of CdTe solar cells with copper (Cu) dopant and atomic layer deposition (ALD) Al_2O_3 with a thickness of 1 nm.[26] The CdTe solar cells based on such an ALD Al_2O_3 layer displays improved efficiency. Despite the previous work with ALD Al_2O_3 to achieve the high performance for CdTe solar cells,[26] the mechanism of ALD Al_2O_3 on the back contact leading to the rectification and tunneling function is still not clear. Herein, we develop a band diagram of the ALD Al_2O_3/Cu_xTe interface in an effort to understand how the ALD Al_2O_3 layer on the CdTe surface improves the performance with the rectification and tunneling effects. We investigate the valence band offset (ΔE_{VBO}) and conduction band offset (ΔE_{CBO}) for the ALD Al_2O_3/Cu_xTe interface by performing X-ray photoelectron spectroscopy (XPS) and first-principles density functional theory calculations. The ALD Al_2O_3/Cu_xTe interface energy band diagram is established and discussed in the terms of CdTe solar cell fabrication.

2. EXPERIMENTAL SECTION

The samples were complete solar-cell structures (without the back contact applied) as shown in Figure 1a; details of experimental conditions were reported in our previous work[26] and the Supporting Information. The XPS measurements were performed by a monochromated Al Kα X-ray source ($h\nu$ = 1486.6 eV) with a vacuum pressure of 1.0×10^{-9} mbar. All core level spectra were recorded with a 0.05 eV step and a 20 eV pass energy. The obtained binding energy (BE) values in the XPS measurements were calibrated by the carbon 1s peak position in the respective sample as reference. BE values of the valence band spectrum of samples were corrected by Au foil mounted along with the samples. The peak contributions were extracted by combining a Lorentzian and a Gaussian function. The background was subtracted using the Shirley function.

3. RESULTS AND DISCUSSION

In the XPS spectra, the zero energy is usually at the Fermi level; nevertheless, charge effect and surface contamination can

Received: June 26, 2016
Accepted: September 23, 2016
Published: September 23, 2016

DOI: 10.1021/acsami.6b07421
ACS Appl. Mater. Interfaces 2016, 8, 28143−28148

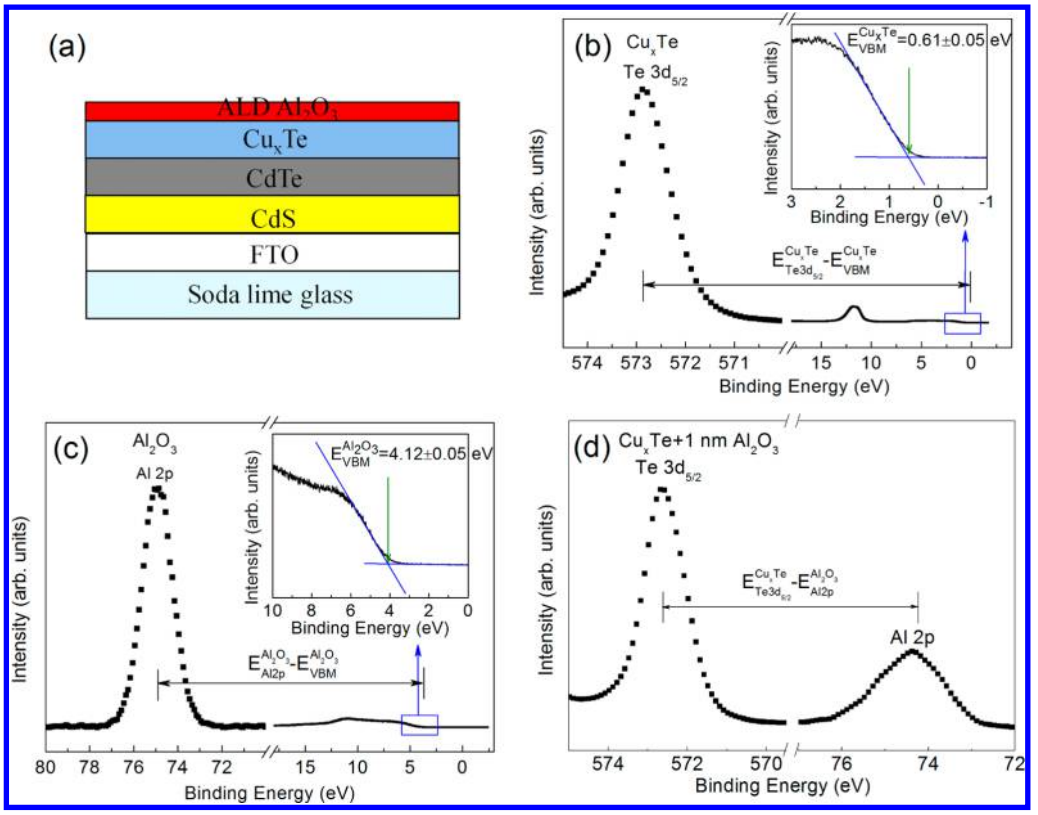

Figure 1. (a) The schematic of the superstrate structure used for CdS/CdTe-based heterojunction solar cells. The core levels, Te $3d_{5/2}$ and Al 2p, and valence band spectra for (b) Cu_xTe layer, (c) 20 nm Al_2O_3 layer, and (d) 1 nm Al_2O_3 layer.

Table 1. Al 2p and Te $3d_{5/2}$ Binding Energies (eV) of the Core Level Spectra for the Cu_xTe Layer, the 20 nm Thick Al_2O_3 Layer, and Different Thickness ALD Al_2O_3 Samples[a]

Al_2O_3 thickness (nm)	0	0.2	0.5	0.8	1	1.5	2	3	20
Al 2p (eV)		74.91	74.80	74.90	74.39	74.36	74.69	74.54	74.93
Te $3d_{5/2}$ (eV)	572.88	572.44	572.41	572.96	572.68	572.48	572.61	572.11	
VBM (eV)	0.61	0.38	0.32	0.26	0.21	0.80	1.31	1.39	4.12
Te $3d_{5/2}$-Al 2p (eV)		497.53	497.61	498.06	498.29	498.12	497.92	497.57	
ΔE_V (eV)		3.93	3.85	3.40	3.19	3.34	3.54	3.89	
E_g (eV)			5.98		4.16	3.85	4.11		
ΔE_C (eV)			1.09		−0.07	−0.53	−0.47		

[a]The valence band maxima (VBM) were recorded for the Cu_xTe layer and the 20 nm thick Al_2O_3 layer. The energy origin is taken at the Fermi level position.

compromise its position. The approach defended here is to use the core level on the samples in order to determine the valence band offset between the Al_2O_3 and Cu_xTe interface. First, considering the mean free path of photoelectrons in a material, a 20 nm Al_2O_3 layer serves as to determine the energy core level (E_{CL}) for bulk Al_2O_3. The same approach is used for Cu_xTe. Lastly, with different thicknesses (0.2−3 nm) of the Al_2O_3 layer, XPS measurement is sensitive to both of Cu_xTe and Al_2O_3, which is consistent with the literatures.[27−29] These samples allow determining the valence band offset.

The valence band offset ΔE_{VBO} values of the ALD Al_2O_3/Cu_xTe interface can be calculated using the equation below[30]

$$\Delta E_{VBO} = (E_{CL} - E_{VBM})_{Cu_xTe} - (E_{CL} - E_{VBM})_{Al_2O_3} - \Delta E_{CL} \quad (1)$$

where $(E_{CL} - E_{VBM})_{Cu_xTe}$ is the difference in binding energy between the Te $3d_{5/2}$ core level and the valence band maximum (VBM) of the Cu_xTe layer. $(E_{CL} - E_{VBM})_{Al_2O_3}$ is the difference in binding energy between the Al $2p_{3/2}$ and VBM value for the 20 nm thick ALD Al_2O_3 film on CdTe. ΔE_{CL} values are the differences in binding energy between Al $2p_{3/2}$ and Te $3d_{5/2}$ core levels for the different thickness ALD Al_2O_3 layers on CdTe, respectively. Because there are no interface reactions occurring, the determination of a valence band offset is accomplished by taking the difference between the Te 3d and Al 2p core levels.[21] Since the calculation of the values for the ALD Al_2O_3/Cu_xTe interfaces are based on the relative energies for each sample, it is necessary to calibrate the spectra.

Figure 1b shows Te $3d_{5/2}$ and valence band spectra of the Cu_xTe layer. The valence band maximum E_{VBM} was obtained by linear fitting to the XPS data. The intersection of the two linear extrapolations corresponds to the valence band maximum, shown in the inset of Figure 1b. The values of E_{VBM} and Te $3d_{5/2}$ measured on a Cu_xTe layer are 0.61 and 572.88 eV, respectively. The corresponding values of E_{VBM} and Al 2p

DOI: 10.1021/acsami.6b07421
ACS Appl. Mater. Interfaces 2016, 8, 28143−28148

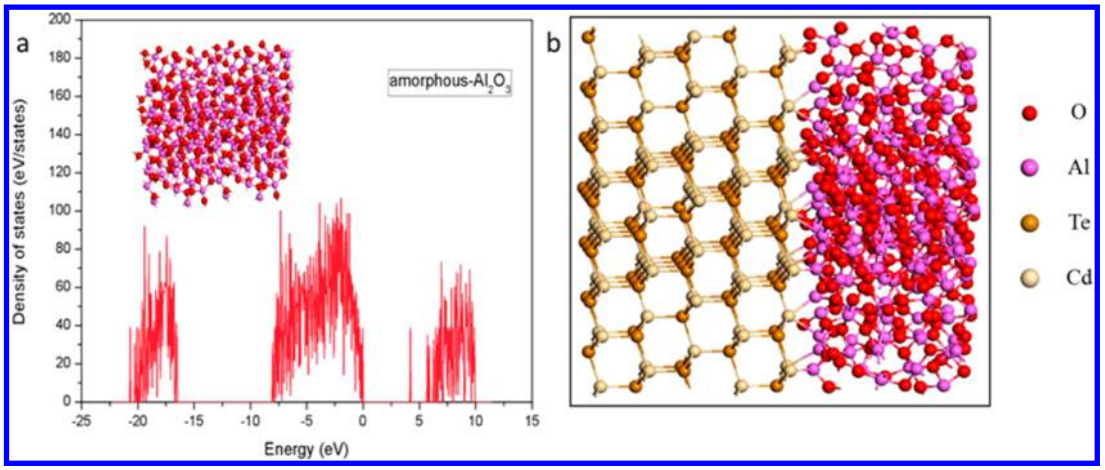

Figure 2. (a) Total density of states of amorphous-Al_2O_3. (b) Relaxed interface of the CdTe/amorphous-Al_2O_3 structure.

measured on a 20 nm thick Al_2O_3 layer are 4.12 and 74.93 eV, respectively, as shown in Figure 1c. ΔE_{CL} is the energy difference between the two core levels of the Al 2p and Te $3d_{5/2}$, which were measured at the ALD Al_2O_3/Cu_xTe interface, as shown in Figure 1d, where the ALD Al_2O_3 thickness was 1 nm. Table 1 summarizes the Al 2p and Te $3d_{5/2}$ binding energies (eV) of the core level spectra for the Cu_xTe layer, the 20 nm Al_2O_3, and Al_2O_3 samples. Using eq 1 and the values reported in Table 1, the valence band offset was calculated for different ALD Al_2O_3 thicknesses (see Table 1). The valence band discontinuity of the ALD Al_2O_3/Cu_xTe interface is represented by ΔE_{VBO}. In order to obtain the conduction band offset ΔE_{CBO}, the band gap of ALD Al_2O_3 is needed.

The band gaps of different thickness ALD Al_2O_3 were predicted through ab initio calculation based on density functional theory (DFT) as implemented in the Vienna Ab-initio Simulation Package (VASP).[31,32] The amorphous-Al_2O_3 structure has been produced using Atomistix ToolKit[33] and optimized by the combination of ab initio molecular dynamic (AIMD) simulation. All of the AIMD simulations to study the interatomic interactions were performed in VASP,[31,32] which is an accurate and effective method for the estimation of the metal oxide structures. The trigonal lattice of the Al_2O_3 structure was converted into new cell by cleaving a 2 × 1 supercell at the [001] surface, resulting in a superlattice of 90 atoms. The low-density structure of Al_2O_3 is obtained by rescaling the periodic boundary conditions of oxide by a factor of 1.2 along every direction. The classical MD simulation for the generation of the amorphous-Al_2O_3 structure began with melting of this rescaled sample at a temperature of 2500 K over 10 000 time steps of 1 fs in the [number of atoms (N), volume (V), and energy (E)] (NVE) ensemble. This high-temperature annealing generates good intermixing of the oxide and completely changes to the disordered structure. After annealing, the sample is again rescaled to the normal density and was cooled down to room temperature in the [number of atoms (N), pressure (P), and temperature (T)] (NPT) Melchionna ensemble at varying temperature intervals with a 1 fs time step and an external stress of 1 bar to obtain the final quenched solid amorphous-Al_2O_3 structure at 300 K. DFT calculations using generalized gradient approximation (GGA) with an exchange correlation function Perdew–Burke–Ernzerhof functional revised for solids (PBE-sol)[34] are used for the energy optimization of the amorphous-Al_2O_3 structure. The electronic wave functions expansion was done at the Γ point of the supercell in plane waves using double-ζ polarized basis set with a cutoff energy of 500 eV. Finally, the structure was allowed to relax until the external pressure and the residual forces on each atom were less than 0.01 kbar and 0.001 eV/Å, respectively. For layer models, we used periodic boundary conditions along the c directions, with vacuum regions of 20 Å between adjacent layers in the direction perpendicular to the layers. Figure 2a shows the amorphous-Al_2O_3 structure and the total DOS and is used further for the generation of the CdTe/amorphous-Al_2O_3 interface as explained in Figure 2b. The band structure of different thickness ALD Al_2O_3 was shown in Figure 3. The result is

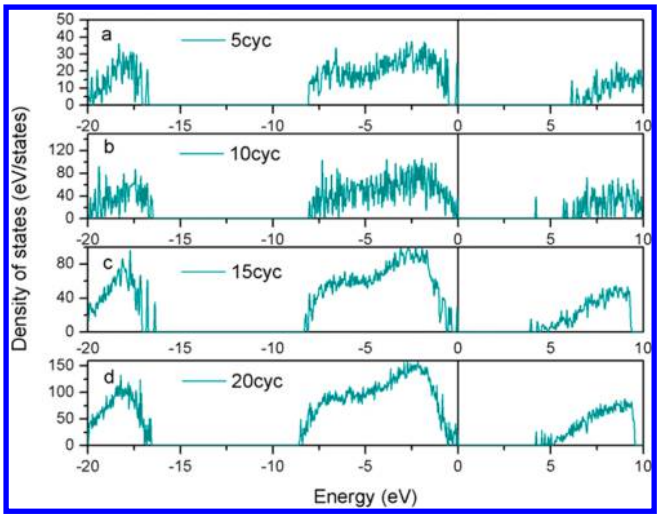

Figure 3. (a) Total density of states of 5cyc-Al_2O_3, (b) 10cyc-Al_2O_3, (c) 15cyc-Al_2O_3, (d) 20cyc-Al_2O_3.

consistent with the literature.[35] The band gap and the VBM of ALD Al_2O_3 change with the thickness were due to the larger interaction volume of the amorphous ALD Al_2O_3.[36]

Taking into account the different thickness ALD Al_2O_3 band gaps and Cu_xTe band gap,[2,3] the energy band diagram of the ALD Al_2O_3/Cu_xTe interface can be established as shown in Figure 4. In our previous work,[26] if the thickness of the ALD Al_2O_3 layer is more than 3 nm, the efficiency shows obvious degradation. This can be explained by the tunneling current, which dominates the charge transportation with the ultrathin (≤ 1 nm) dielectrics of Al_2O_3, but a thick film (> 1 nm) would block the charge transportation. The back contact with 1 nm

DOI: 10.1021/acsami.6b07421
ACS Appl. Mater. Interfaces 2016, 8, 28143–28148

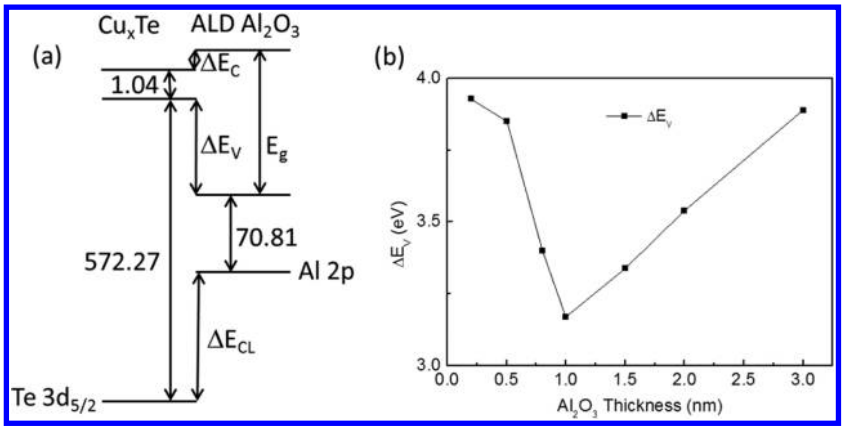

Figure 4. (a) Energy band diagram of the ALD Al_2O_3/Cu_xTe interface. The valence and conduction band offsets are represented. Also indicated are the differences in energy between core levels and valence band maxima for Al_2O_3 and Cu_xTe as well as the difference in core level energy ΔE_{CL}. (b) Valence band offsets ΔE_{VBO} for different thickness ALD Al_2O_3 samples.

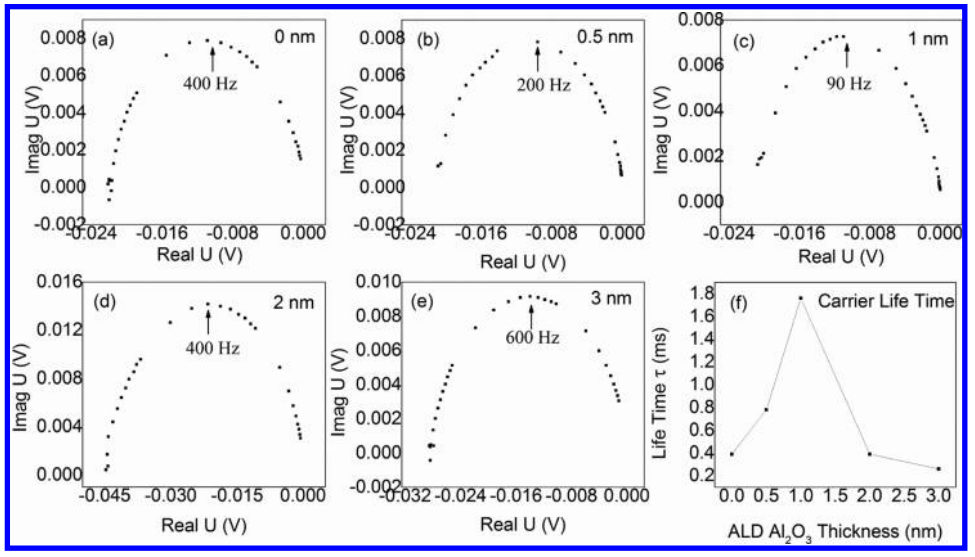

Figure 5. IMVS response of the samples with ALD-Al_2O_3 of (a) 0, (b) 0.5 nm, (c) 1 nm, (d) 2 nm, (e) 3 nm. (f) The carrier lifetime τ versus the ALD Al_2O_3 thickness.

ALD Al_2O_3 has the improved efficiency, up to 12.1%, compared with the efficiency of 10.7% without ALD Al_2O_3 modification.[26] In order to quantitatively evaluate the enhancement of carriers lifetime by ALD Al_2O_3 passivation, small-amplitude intensity-modulated photovoltage spectroscopy (IMVS) was measured under a 560 nm light source with the structure of FTO/CdS/CdTe/Cu/Al_2O_3/Au (see Figure 5a–e). IMVS was used to investigate the recombination processes. The IMVS plots display a semicircle in the complex plane. The carrier lifetime (τ) can be estimated from the $\tau = (2\pi f_{max})^{-1}$,[37−39] where τ is the carrier lifetime and f_{max} is the max response frequency at the IMVS plots. Figure 5 shows complex plane plots of the IMVS spectrum for CeTe solar cells and the time constant τ. The shorter carrier lifetime indicates that more recombination sites exist in CdTe solar cells without the ALD Al_2O_3 layer. The fast recombination rate could be the main reason for the decreasing of PCE. It can be observed from Figure 5f that the best τ is achieved in the sample with 1 nm ALD Al_2O_3.

The tunneling probability (T) using a semiclassical theory of tunneling through a finite square potential barrier is

$$T = [1 + C \sinh^2(\kappa d)]^{-1} \quad (2)$$

where C is a parameter related to the carrier energy, d is the thickness of Al_2O_3, and $\kappa = \sqrt{2m^*\Delta}/\hbar$ (m^* is the effective mass of carrier and Δ is the barrier height). From Figure 4b, the valence band offset ΔE_{VBO} has the minimum value (3.19 eV) for the 1 nm ALD Al_2O_3 layer sample. As a result, the CdTe solar cell with 1 nm ALD Al_2O_3 has the smallest potential barrier for hole carries. As the thickness of ALD Al_2O_3 is larger than 1 nm, the charge transportation would be blocked. This is in accordance with the photocurrent $J-V$ characteristics with the best FF in the 1 nm Al_2O_3 sample. The mechanism could include two factors. First, the Al_2O_3 insulator with a thickness less than 1 nm not only facilitates large tunneling for hole carriers but also blocks minority carriers (electron) in the positive pole. Second, the thickness of above 3 nm would block the hole transportation. Only if the thickness of Al_2O_3 is around 1 nm does the modification layer function to allow the channeling of holes, but blocks the transportation of electrons. Therefore, the CdTe solar cell with 1 nm ALD Al_2O_3 modification has the optimized efficiency.

DOI: 10.1021/acsami.6b07421
ACS Appl. Mater. Interfaces 2016, 8, 28143−28148

4. CONCLUSIONS

In conclusion, the energy diagram of the ALD Al_2O_3/Cu_xTe interface can be established by combining experiments and first-principles calculations. The mechanism of the improved performance of the CdTe solar cells with ALD Al_2O_3 modification due to the rectification and tunneling function is discussed. The interfacial energy band diagram configuration of the ALD Al_2O_3/Cu_xTe band alignment with optimized layer thickness (about 1 nm ALD Al_2O_3) is the key factor for rectification and tunneling effects.

■ ASSOCIATED CONTENT

Supporting Information

The Supporting Information is available free of charge on the ACS Publications website at DOI: 10.1021/acsami.6b07421.

The procedure details for fabrication of CdTe solar cells (PDF)

■ AUTHOR INFORMATION

Corresponding Author

*E-mail: panfeng@pkusz.edu.cn.

Author Contributions

†These authors contributed equally.

Notes

The authors declare no competing financial interest.

■ ACKNOWLEDGMENTS

This work was financially supported by NSFC (Grant Nos. 11404011 and 51302007), Guangdong Innovative and Entrepreneurial Research Team Program (Grant No. 2013N080), Guangdong Natural Science Funds for Distinguished Young Scholar (Grant No. 2015A030306036), and Shenzhen Science and Technology Innovation Committee (Grant Nos. JCYJ20150331100515911, JCYJ20150629144835001, JCYJ20140417144423201, Peacock Plan KQCX20150327093155293, and Peacock Plan KYPT20141016105435850).

■ REFERENCES

(1) Wu, X. High-Efficiency Polycrystalline CdTe Thin-Film Solar Cells. *Sol. Energy* **2004**, *77*, 803−814.

(2) Kranz, L.; Gretener, C.; Perrenoud, J.; Schmitt, R.; Pianezzi, F.; La Mattina, F.; Blosch, P.; Cheah, E.; Chirila, A.; Fella, C. M.; Hagendorfer, H.; Jager, T.; Nishiwaki, S.; Uhl, A. R.; Buecheler, S.; Tiwari, A. N. Doping of Polycrystalline CdTe for High-Efficiency Solar Cells on Flexible Metal Foil. *Nat. Commun.* **2013**, *4*, 2306.

(3) Green, M. A.; Emery, K.; Hishikawa, Y.; Warta, W.; Dunlop, E. D. Solar Cell Efficiency Tables (Version 45). *Prog. Photovoltaics* **2015**, *23*, 1−9.

(4) Fedorenko, Y. G.; Major, J. D.; Pressman, A.; Phillips, L. J.; Durose, K. Modification of Electron States in CdTe Absorber due to a Buffer Layer in CdTe/CdS Solar Cells. *J. Appl. Phys.* **2015**, *118*, 165705.

(5) Mughal, M. A.; Engelken, R.; Sharma, R. Progress in Indium (III) Sulfide (In_2S_3) Buffer Layer Deposition Techniques for CIS, CIGS, and CdTe-Based Thin Film Solar Cells. *Sol. Energy* **2015**, *120*, 131−146.

(6) Stechmann, G.; Zaefferer, S.; Konijnenberg, P.; Raabe, D.; Gretener, C.; Kranz, L.; Perrenoud, J.; Buecheler, S.; Tiwari, A. N. 3-Dimensional Microstructural Characterization of CdTe Absorber Layers from CdTe/CdS Thin Film Solar Cells. *Sol. Energy Mater. Sol. Cells* **2016**, *151*, 66−80.

(7) Williams, B. L.; Major, J. D.; Bowen, L.; Keuning, W.; Creatore, M.; Durose, K. A Comparative Study of the Effects of Nontoxic Chloride Treatments on CdTe Solar Cell Microstructure and Stoichiometry. *Adv. Energy Mater.* **2015**, *5*, 1500554.

(8) Zeng, Q.; Chen, Z.; Zhao, Y.; Du, X.; Liu, F.; Jin, G.; Dong, F.; Zhang, H.; Yang, B. Aqueous-Processed Inorganic Thin-Film Solar Cells Based on $CdSe_xTe_{1-x}$ Nanocrystals: The Impact of Composition on Photovoltaic Performance. *ACS Appl. Mater. Interfaces* **2015**, *7*, 23223−23230.

(9) Sardashti, K.; Haight, R.; Gokmen, T.; Wang, W.; Chang, L.-Y.; Mitzi, D. B.; Kummel, A. C. Impact of Nanoscale Elemental Distribution in High-Performance Kesterite Solar Cells. *Adv. Energy Mater.* **2015**, *5*, 1402180.

(10) Reese, M. O.; Perkins, C. L.; Burst, J. M.; Farrell, S.; Barnes, T. M.; Johnston, S. W.; Kuciauskas, D.; Gessert, T. A.; Metzger, W. K. Intrinsic Surface Passivation of CdTe. *J. Appl. Phys.* **2015**, *118*, 155305.

(11) Duncan, D. A.; Kephart, J. M.; Horsley, K.; Blum, M.; Mezher, M.; Weinhardt, L.; Haming, M.; Wilks, R. G.; Hofmann, T.; Yang, W.; Bar, M.; Sampath, W. S.; Heske, C. Characterization of Sulfur Bonding in CdS:O Buffer Layers for CdTe-based Thin-Film Solar Cells. *ACS Appl. Mater. Interfaces* **2015**, *7*, 16382−16386.

(12) Corwine, C. Copper Inclusion and Migration from the Back Contact in CdTe Solar Cells. *Sol. Energy Mater. Sol. Cells* **2004**, *82*, 481−489.

(13) Demtsu, S. H.; Sites, J. R. Effect of Back-Contact Barrier on Thin-Film CdTe Solar Cells. *Thin Solid Films* **2006**, *510*, 320−324.

(14) Pan, J.; Gloeckler, M.; Sites, J. R. Hole Current Impedance and Electron Current Enhancement by Back-Contact Barriers in CdTe Thin Film Solar Cells. *J. Appl. Phys.* **2006**, *100*, 124505.

(15) Drayton, J. A.; Williams, D. D.; Geisthardt, R. M.; Cramer, C. L.; Williams, J. D.; Sites, J. R. Molybdenum Oxide and Molybdenum Oxide-Nitride Back Contacts for CdTe Solar Cells. *J. Vac. Sci. Technol., A* **2015**, *33*, 041201.

(16) Matin, M. A.; Mannir Aliyu, M.; Quadery, A. H.; Amin, N. Prospects of Novel Front and Back Contacts for High Efficiency Cadmium Telluride Thin Film Solar Cells from Numerical Analysis. *Sol. Energy Mater. Sol. Cells* **2010**, *94*, 1496−1500.

(17) Kumar, S. G.; Rao, K. S. R. K. Physics and Chemistry of CdTe/CdS Thin Film Heterojunction Photovoltaic Devices: Fundamental and Critical Aspects. *Energy Environ. Sci.* **2014**, *7*, 45−102.

(18) Lin, H.; Xia, W.; Wu, H. N.; Tang, C. W. CdS/CdTe Solar Cells with MoO_x as Back Contact Buffers. *Appl. Phys. Lett.* **2010**, *97*, 123504.

(19) Liang, J.; Bi, H.; Wan, D. Y.; Huang, F. Q. Novel Cu Nanowires/Graphene as the Back Contact for CdTe Solar Cells. *Adv. Funct. Mater.* **2012**, *22*, 1267−1271.

(20) Phillips, A. B.; Khanal, R. R.; Song, Z.; Zartman, R. M.; DeWitt, J. L.; Stone, J. M.; Roland, P. J.; Plotnikov, V. V.; Carter, C. W.; Stayancho, J. M.; Ellingson, R. J.; Compaan, A. D.; Heben, M. J. Wiring-Up Carbon Single Wall Nanotubes to Polycrystalline Inorganic Semiconductor Thin Films: Low-Barrier, Copper-Free Back Contact to CdTe Solar Cells. *Nano Lett.* **2013**, *13*, 5224−5232.

(21) Hoex, B.; Heil, S. B. S.; Langereis, E.; van de Sanden, M. C. M.; Kessels, W. M. M. Ultralow Surface Recombination of c-Si Substrates Passivated by Plasma-Assisted Atomic Layer Deposited Al_2O_3. *Appl. Phys. Lett.* **2006**, *89*, 042112.

(22) Poodt, P.; Lankhorst, A.; Roozeboom, F.; Spee, K.; Maas, D.; Vermeer, A. High-Speed Spatial Atomic-Layer Deposition of Aluminum Oxide Layers for Solar Cell Passivation. *Adv. Mater.* **2010**, *22*, 3564−3567.

(23) Dingemans, G.; Beyer, W.; van de Sanden, M. C. M.; Kessels, W. M. M. Hydrogen Induced Passivation of Si Interfaces by Al_2O_3 Films and SiO_2/Al_2O_3 Stacks. *Appl. Phys. Lett.* **2010**, *97*, 152106.

(24) Werner, F.; Veith, B.; Zielke, D.; Kühnemund, L.; Tegenkamp, C.; Seibt, M.; Brendel, R.; Schmidt, J. Electronic and Chemical Properties of the c-Si/Al_2O_3 Interface. *J. Appl. Phys.* **2011**, *109*, 113701.

(25) Meinander, K.; Preston, J. S. A DFT Study on the Effect of Surface Termination in CdTe (111)/α-Al_2O_3 (0001) Heteroepitaxy. *Surf. Sci.* **2015**, *632*, 93−97.

DOI: 10.1021/acsami.6b07421
ACS Appl. Mater. Interfaces 2016, 8, 28143−28148

(26) Liang, J.; Lin, Q. X.; Li, H.; Su, Y. T.; Yang, X. Y.; Wu, Z. Z.; Zheng, J. X.; Wang, X. W.; Lin, Y.; Pan, F. Rectification and Tunneling Effects Enabled by Al_2O_3 Atomic Layer Deposited on Back Contact of CdTe Solar Cells. *Appl. Phys. Lett.* **2015**, *107*, 013907.
(27) Maréchal, A.; Aoukar, M.; Vallée, C.; Rivière, C.; Eon, D.; Pernot, J.; Gheeraert, E. Energy-Band Diagram Configuration of Al_2O_3/Oxygen-Terminated p-Diamond Metal-Oxide-Semiconductor. *Appl. Phys. Lett.* **2015**, *107*, 141601.
(28) King, S. W.; Nemanich, R. J.; Davis, R. F. Band Alignment at AlN/Si(111) and (001) Interfaces. *J. Appl. Phys.* **2015**, *118*, 045304.
(29) Liu, X.; He, J.; Liu, Q.; Tang, D.; Jia, F.; Wen, J.; Lu, Y.; Yu, W.; Zhu, D.; Liu, W.; Cao, P.; Han, S.; Pan, J.; He, Z.; Ang, K.-W. Band Alignment of HfO_2/Multilayer MoS_2 Interface Determined by X-ray Photoelectron Spectroscopy: Effect of CHF_3 Treatment. *Appl. Phys. Lett.* **2015**, *107*, 101601.
(30) Kraut, E. A.; Grant, E. W.; Waldrop, J. R.; Kowalczyk, S. P. Precise Determination of the Valence-Band Edge in X-Ray Photoemission Spectra: Application to Measurement of Semiconductor Interface Potentials. *Phys. Rev. Lett.* **1980**, *44*, 1620.
(31) Kresse, G.; Furthmüller, J. Efficient Iterative Schemes for ab Initio Total-Energy Calculations Using a Plane-Wave Basis Set. *Phys. Rev. B: Condens. Matter Mater. Phys.* **1996**, *54*, 11169−11186.
(32) Kresse, G.; Joubert, D. From Ultrasoft Pseudopotentials to the Projector Augmented-Wave Method. *Phys. Rev. B: Condens. Matter Mater. Phys.* **1999**, *59*, 1758.
(33) *Atomistix ToolKit*, v.14.3; Quantumwise: Copenhagen, Denmark, 2015. http://quantumwise.com/ (accessed 2015).
(34) Perdew, J. P.; Burke, K.; Ernzerhof, M. Generalized Gradient Approximation Made Simple. *Phys. Rev. Lett.* **1996**, *77*, 3865−3868.
(35) Bansal, A.; Mishra, H.; Bhattacharya, S.; Singh, B. R. First Principles Calculations of Bonding and Charges at the Al_2O_3 Interfaces in a c-Si/SiO_2/am-Al_2O_3 Structure Applicable. *IEEE Trans. Electron Devices* **2016**, *63*, 544−550.
(36) Schulz, P.; Dowgiallo, A.-M.; Yang, M.; Zhu, K.; Blackburn, J. L.; Berry, J. J. Charge Transfer Dynamics Between Carbon Nanotubes and Hybrid Organic Metal Halide Perovskite Films. *J. Phys. Chem. Lett.* **2016**, *7*, 418−425.
(37) Krüger, J.; Plass, R.; Grätzel, M.; Cameron, P. J.; Peter, L. M. Charge Transport and Back Reaction in Solid-State Dye-Sensitized Solar Cells: A Study Using Intensity-Modulated Photovoltage and Photocurrent Spectroscopy. *J. Phys. Chem. B* **2003**, *107*, 7536−7539.
(38) Duan, Y. D.; Zheng, J. X.; Fu, N. Q.; Fang, Y. Y.; Liu, T. C.; Zhang, Q.; Zhou, X. W.; Lin, Y.; Pan, F. Enhancing the Performance of Dye-Sensitized Solar Cells: Doping SnO_2 Photoanodes with Al to Simultaneously Improve Conduction Band and Electron Lifetime. *J. Mater. Chem. A* **2015**, *3*, 3066−3073.
(39) Duan, Y. D.; Zheng, J. X.; Xu, M.; Song, X. H.; Fu, N. Q.; Fang, Y. Y.; Zhou, X. W.; Lin, Y.; Pan, F. Metal and F Dual-Doping to Synchronously Improve Electron Transport Rate and Lifetime for TiO_2 Photoanode to Enhance Dye-Sensitized Solar Cells Performances. *J. Mater. Chem. A* **2015**, *3*, 5692−5700.

DOI: 10.1021/acsami.6b07421
ACS Appl. Mater. Interfaces 2016, 8, 28143−28148